THYROID
Volume 23, Number 11, 2013

DOI: 10.1089/thy.2012.0243

Morphometric and Functional Changes of Salivary Gland Dysfunction After Radioactive Iodine Ablation in a Murine Model

Jeong-Seok Choi,[1] In Suh Park,[2] Seok-Ki Kim,[3] Jae-Yol Lim,[1,*] and Young-Mo Kim[1,*]

Background: Ablation of the thyroid tissue using radioactive iodine (RAI) after the surgical removal of well-differentiated thyroid cancer can induce radiation-related salivary gland (SG) dysfunction. However, *in vivo* changes of SGs after RAI administration in appropriate animal models are not well described in the literature. This study was undertaken to document morphometric and functional changes during the 12 months after RAI administration in a murine model of RAI-induced SG dysfunction.
Methods: Four-week-old female C57BL/6 mice ($n=60$) were divided into an RAI-treated group ($n=30$) that received RAI orally (0.01 mCi/g body weight) and an unexposed control group ($n=30$). Mice in both groups were divided into five subgroups ($n=6$ per subgroup) and euthanized at 1, 2, 3, 6, and 12 months post-RAI administration. Salivary flow rates and salivary lag times were measured at 1, 2, 3, 6, and 12 months after RAI administration. Morphological and histological examinations and terminal deoxynucleotidyl transferase dUTP nick end labeling assays were performed. In addition, changes in salivary ^{99m}Tc pertechnetate uptake and excretion were observed by single-photon emission computed tomography.
Results: In RAI-treated mice, the SGs were significantly lighter than those of unexposed controls at all study time points. Lag times to salivation in the RAI-treated group were greater than in the unexposed controls, but mean salivary flow rates were lower. Histologic examinations of SGs in the RAI group showed pale cytoplasm, atypical ductal configuration, septal widening, cytoplasmic vacuolization with pleomorphism, lymphocyte infiltration, and increased fibrosis. Furthermore, more apoptotic cells were observed in acini and ducts in the RAI group. In addition, patterns of ^{99m}Tc pertechnetate uptake and excretion in the RAI group were quite different from those observed in controls at 1 and 12 months post-RAI.
Conclusion: Various histological alterations were observed in mice exposed to RAI, that is, an increase in apoptotic acini and ductal cells and functional SG deterioration. The murine model of RAI-induced SG dysfunction used in the present study appears to be applicable to preclinical research on RAI-induced sialadenitis in patients with well-differentiated thyroid cancer.

Introduction

Radioactive iodine (RAI) ablation is performed to detect and remove remnant thyroid tissue in patients who have undergone total thyroidectomy for well-differentiated thyroid cancer. After RAI therapy, patients often complain of painful swelling of salivary glands (SGs), xerostomia, taste alterations, or oral infections (1–4). Furthermore, RAI therapy increases the risks of caries and tooth extraction (5), and SG dysfunction induced by RAI impairs long-term oral health and quality of life.

However, the *in vivo* SG changes induced by RAI administration in an appropriate animal model have not been well described in the literature. In this study, we investigated morphometric and functional changes that occurred during the 12 months after RAI administration in a murine model of RAI-induced SG dysfunction. During the study, we measured (i) changes in body weight, (ii) changes in SG weights, and (iii) salivary lag times (times from pilocarpine administration until commencement of salivary flow) and salivary flow rates (SFRs), and performed (iv) histopathologic examinations, (v) terminal deoxynucleotidyl transferase dUDP nick

Departments of [1]Otorhinolaryngology–Head and Neck Surgery and [2]Pathology, Inha University School of Medicine, Incheon, Republic of Korea.
[3]Department of Nuclear Medicine, National Cancer Center, Goyang-si, Republic of Korea.
*These two authors contributed equally to this work.

end labeling (TUNEL) assays to detect apoptosis, and (vi) single-photon emission computed tomography (SPECT) to evaluate changes in ^{99m}Tc pertechnetate salivary uptake and excretion rates.

Materials and Methods

Animal studies

Sixty female, 4-week-old, C57BL/6 mice weighing 18–22 g were obtained from the Animal House Facility, National Cancer Research Center, and maintained under temperature- and light-controlled conditions in an animal facility with free access to water and a standard mouse diet. Animal studies were performed in compliance with the National Cancer Research Center Institutional Animal Ethics Committee's guidelines.

RAI was not administered to group A (unexposed control group, $n=30$). Group B (RAI-treated group, $n=30$) received RAI intraorally (0.01 mCi/g body weight, ^{131}I; New Korea Industrial). RAI administration was defined to occur on day 0. Both groups were then divided into five subgroups ($n=6$ per subgroup) and euthanized at 1, 2, 3, 6, and 12 months post-treatment, respectively.

Measurements of mouse body weights, SG weights, salivary lag times, and SFRs

Mice were weighed, and administered ketamine (100 mg/kg) and xylazine (5 mg/kg) in sterile water intraperitoneally (i.p.). Pilocarpine (2 mg/kg body weight; i.p.) was then administered. Saliva was collected for 5 minutes after pilocarpine administration using a specifically designed suction device and placed in a preweighed 0.75 mL Eppendorf tube. SFR (μL/min) was defined as the total saliva weight (mg) divided by the collection time (min) (saliva was assumed to have a specific gravity of 1 mg/mL). Salivary lag time was defined as time from stimulation to the commencement of saliva secretion. After saliva collection and euthanasia, submaxillary glands were harvested and surrounding fat and connective tissues were removed. Both submaxillary glands were weighed.

Morphological analysis of tissues and TUNEL assay

SGs were immediately placed in 4% paraformaldehyde at room temperature, processed, embedded in paraffin, sectioned at 4 μm, and stained with hematoxylin and eosin and Masson's Trichrome.

Apoptosis in SG tissues was quantified by the TUNEL assay using an ApopTag Plus In Situ Apoptosis Kit (Chemicon Int.) at 2, 6, and 12 months post-RAI administration. TUNEL-positive cells were detected at 400×, and two blinded examiners independently counted the numbers of apoptotic cells in three random fields per tissue section.

SPECT protocol

Technetium pertechnetate (55.5 MBq, [^{99m}Tc] TcO_4^-; New Korea Industrial) was administered i.p. to the anesthetized mice. The mice were maintained in an unconscious state during the entire imaging protocol using isoflurane (2 vol.% in air). Whole-body SPECT imaging was started immediately after [^{99m}Tc]TcO_4^- injection and was repeated every 5–100 minutes (NanoSPECT; Bioscan). Overall, 21 images were obtained per mouse. Pilocarpine (2 mg/kg body weight; i.p.) was administered at 60 minutes post-SPECT. Each mouse was imaged at 1 and 12 months post-RAI.

Whole-body SPECT protocol

Whole-body SPECT images of each mouse were obtained using a large field-of-view rotating gamma camera equipped with four multipinhole collimators (Fig. 1A, B). The acquisition parameters used were as follows: 24 projections over 360°, a circular orbit, and a total acquisition time of 6 minutes (4 seconds per projection). Tomographic images were reconstructed using an iterative reconstruction algorithm) (6,7).

SPECT image analysis

SPECT images were reviewed and quantified using In Vivo Scope (Bioscan) and Osirix (The Osirix Foundation) imaging software. Regions of interest were drawn manually around

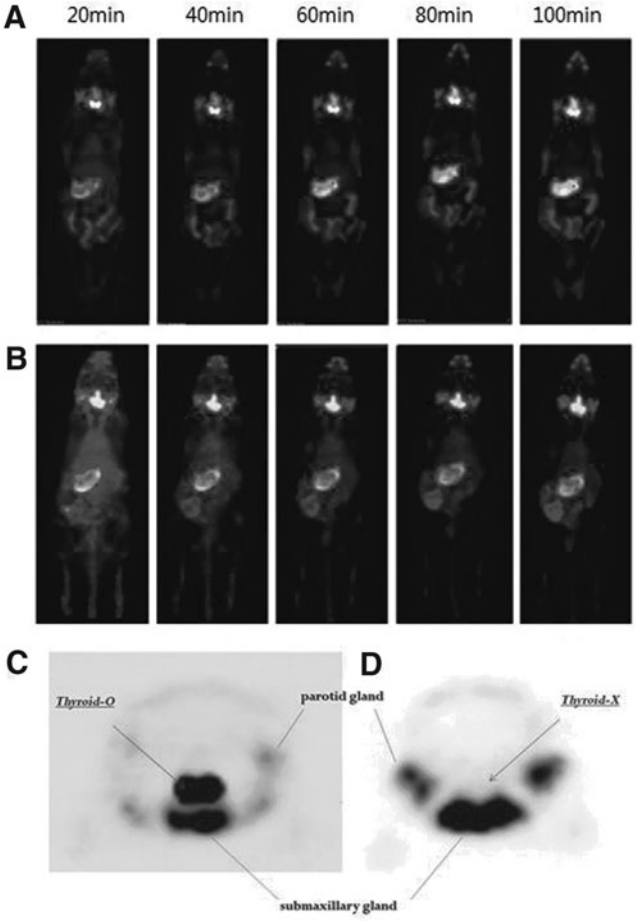

FIG. 1. Planar whole-body images of **(A)** an unexposed control mouse and **(B)** an RAI-administered mouse, and neck transaxial planar images of **(C)** an unexposed control mouse and **(D)** an RAI-treated mouse. Whole-body imaging was performed in anterior view using a pinhole 10 cm removed from target mice. Thyroid tissue was not imaged by neck transaxial planar imaging in RAI-administered mice because of the ablative effects of treatment after 1 month. RAI, radioactive iodine.

the thyroid and SGs on images obtained 60 minutes post-contrast administration that best depicted thyroid and SG contours. Regions of interest of each lesion were combined into a volume of interest (VOI), and VOIs were copied and pasted onto SPECT images, except for images obtained at 60 minutes post-contrast administration. In addition, all VOIs were corrected to ensure that they did not contain counts from neighboring tissues, such as bone (Fig. 2C, D). The radioactivity values of all voxels in VOIs were measured and corrected for activity decay post-treatment. We used maximal normalized radioactivity in VOIs as representative values to minimize partial-volume effects. No thyroid tissue was imaged in the RAI-treated mice. We attribute this to RAI ablation of thyroid tissues.

Statistical analysis

Data were analyzed using GraphPad Prism 5 package (GraphPad Software Inc.). The significances of differences between groups were determined using the Student's *t*-test and two-way analysis of variance. Differences were accepted to be statistically significant at $p < 0.05$. All results are expressed as means ± standard deviations.

Results

Changes in body and SG weights

At baseline, no significant weight difference was observed between the RAI-treated group and the unexposed control group ($p = 0.54$). However, at 1, 2, and 12 months post-RAI administration, mice in the RAI-treated group weighed significantly less than mice in the unexposed control group ($p < 0.01$, $p = 0.04$, and $p = 0.03$, respectively) (Fig. 2A). SGs of RAI-treated mice also weighed significantly less than those of unexposed control mice at 1, 2, 3, and 6 months ($p = 0.04$, $p < 0.01$, $p = 0.02$, and $p = 0.01$, respectively) (Fig. 2B). Reductions in SG weight were greater than reductions in body weight in RAI-treated mice than in unexposed control mice at 1, 2, 3, 6, and 12 months, and differences were statistically significant at 2 and 3 months ($p < 0.001$ and $p < 0.05$, respectively).

Salivary lag times and SFRs

No significant intergroup difference was observed between salivary lag times at 1 ($p = 0.44$) or 2 months ($p = 0.79$), but mean lag times in the RAI-treated group were greater than those in the unexposed control group between 3 and 12

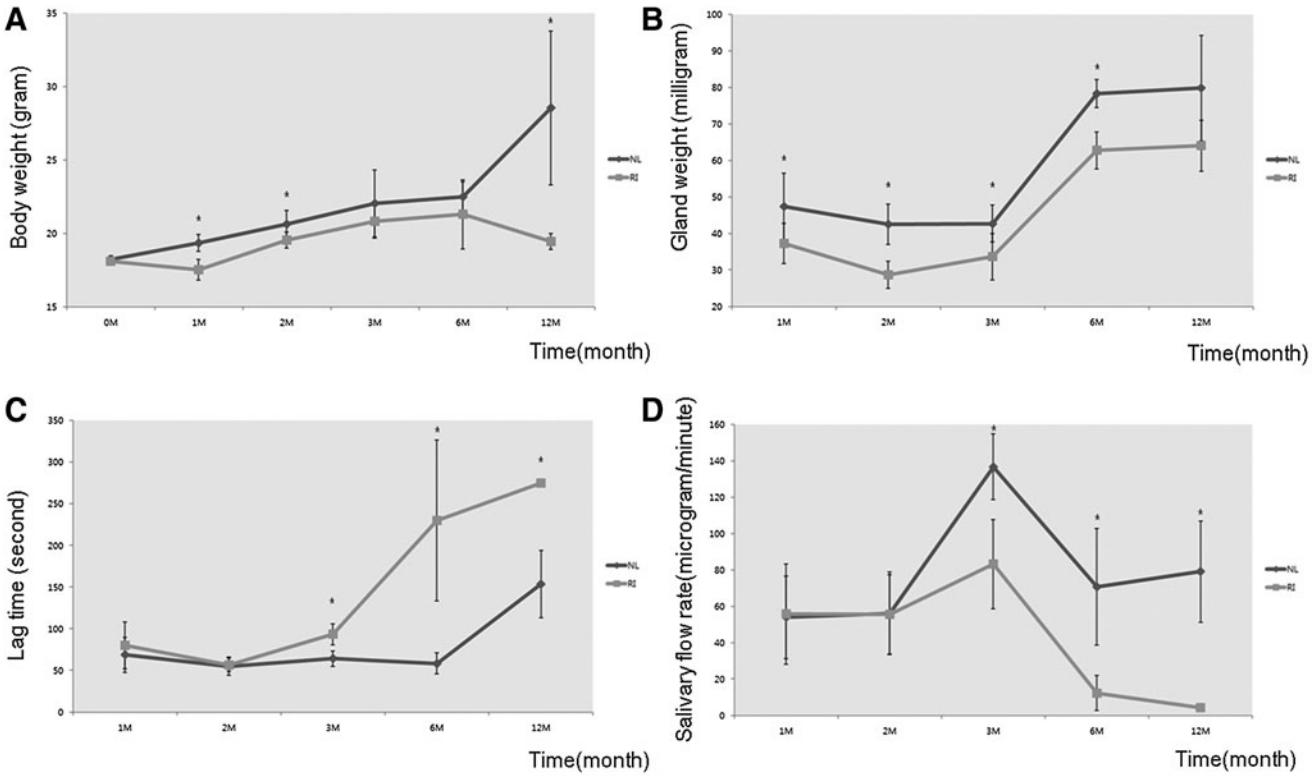

FIG. 2. **(A)** Comparison of mouse weights. Mice in the RAI-treated group weighed less than mice in the unexposed control group at 1 month post-treatment, and significantly less than mice in the unexposed control group at 1, 2, and 12 months post-treatment ($p < 0.001$). **(B)** Comparison of SG weights. SGs weighed less in the RAI-treated group than in the unexposed control group from 1 to 12 months post-treatment, and these differences were significant at 1, 2, 3, and 6 months ($p < 0.001$). **(C)** Comparison of salivary lag times. No significant intergroup difference in lag times was observed at 1 or 2 months post-treatment. However, mean lag times in the RAI-treated group were significantly greater from 3 to 12 months ($p < 0.001$). **(D)** Comparison of SFRs. No significant intergroup difference in SFRs was observed at 1 or 2 months post-treatment, but the mean SFRs in the RAI-treated group were significantly smaller than those in the unexposed control group at 3–12 months post-treatment ($p < 0.001$). **(A–D)** Dots and error bars denote means ± standard deviations; *x*-axis denotes months (M); asterisks indicate statistically significant points (NL, normal unexposed control group; RAI, RAI-treated group). SG, salivary gland; SFRs, salivary flow rates.

months ($p < 0.01$, $p = 0.04$, and $p < 0.01$, respectively) (Fig. 2C). In addition, no significant difference between mean SFR values was observed at 1 ($p = 0.91$) or 2 months ($p = 0.97$). Mean SFR in the RAI-treated group was less than that in the unexposed control group at 3–12 months ($p < 0.01$, $p = 0.04$, and $p < 0.01$, respectively) (Fig. 2D).

Evaluation of histological changes and apoptosis

No significant pathologic changes were observed in RAI-treated SGs at 1 or 2 months. RAI-treated SGs exhibited pale cytoplasm (Fig. 3B), atypical ductal configuration (Fig. 3C), septal widening (Fig. 3D), and lymphocyte infiltration (Fig. 3E) at 6 months, and cytoplasmic vacuolization with pleomorphism (Fig. 3F) at 3 months as compared with unexposed SGs (Fig. 3A). Furthermore, Masson's Trichrome staining of RAI-treated SGs revealed higher levels of fibrosis (Fig. 3G, H).

TUNEL assays showed that the number of apoptotic acinar cells was significantly higher in the RAI-treated group at 2, 6, and 12 months ($p = 0.04$, $p = 0.05$, and $p < 0.01$, respectively) (Fig. 4A). Similarly, numbers of apoptotic ductal cells were significantly higher in the RAI-treated group at 2 and 12 months ($p < 0.01$ and $p < 0.01$, respectively) (Fig. 4B).

SPECT: Dynamics of ^{99m}Tc pertechnetate uptake and excretion at 1 and 12 months post-treatment

The rate of ^{99m}Tc pertechnetate uptake in unexposed controls was greater than that in RAI-treated mice, and the ^{99m}Tc pertechnetate excretion amount was markedly lower in RAI-treated mice at 1 month post-RAI administration (Fig. 5A). The rate of ^{99m}Tc pertechnetate uptake in RAI-treated mice was lower than that in unexposed control mice, but the amount of ^{99m}Tc pertechnetate excretion was similar in the two groups at 12 months post-RAI (Fig. 5B).

Discussion

In recent years, RAI therapy after total thyroidectomy has played an important role in the treatment of patients with well-differentiated thyroid cancer. Ideally, this treatment should ablate residual tumor cells in the neck and distant metastases, but not affect surrounding healthy tissues (8). However, RAI affects many nonthyroidal tissues, such as SGs, lacrimal glands, gastric mucosa, lactating mammary glands, placenta, thymus, lung, and bone marrow (9,10), because all these tissues express the sodium iodide symporter (NIS). NIS is an integral plasma membrane glycoprotein that mediates the active transport of iodide ions into thyroid follicular cells (11–13) and thus plays a major role in RAI uptake. As a result, RAI can accumulate in SG tissues because of the action of native NIS (14,15).

RAI-induced SG dysfunction, which may be transient or permanent, impairs quality of life (5). Furthermore, because patients with differentiated thyroid cancer have a good prognosis, it is critical to minimize the side effects of RAI therapy; for this reason, the protection of SGs after RAI therapy has become an important issue.

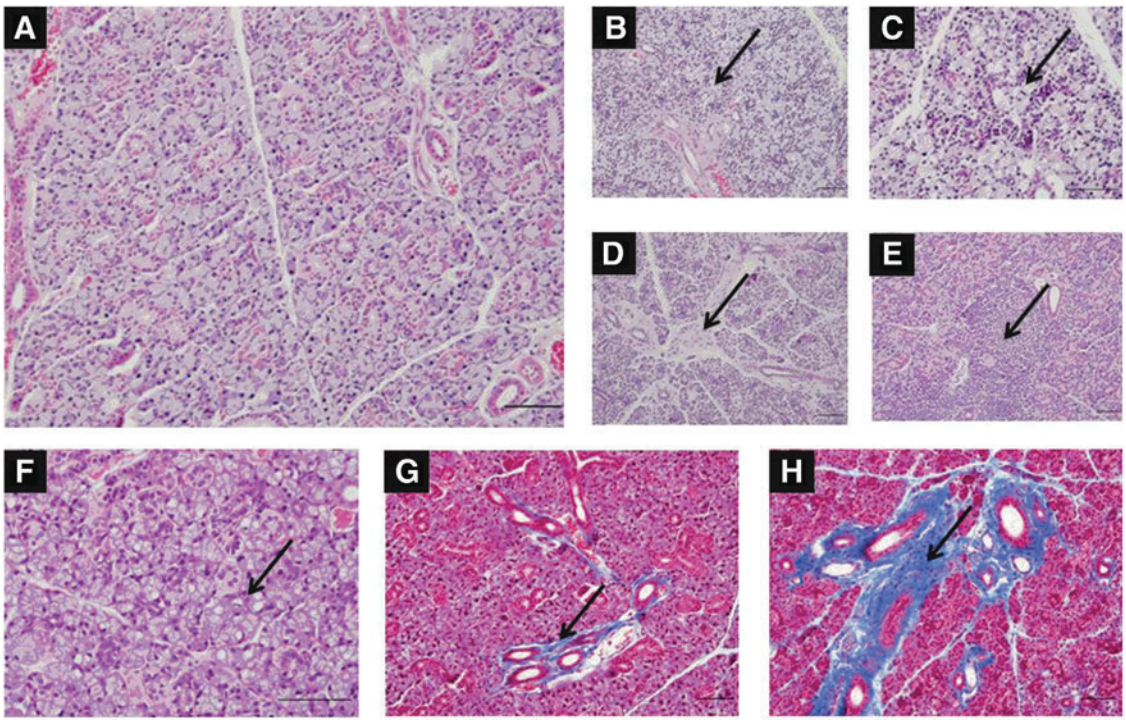

FIG. 3. Histological analysis of representative samples. Histological analysis of normal SGs (submaxillary glands) revealed the expected lobular structure with densely packed acini and a well-developed excretory duct system. **(A)** An unexposed control at 12 months; **(B)** pale cytoplasm in an RAI-administered mouse at 12 months; **(C)** an atypical ductal configuration in an RAI-administered mouse at 12 months; **(D)** septal widening in an RAI-administered mouse at 12 months; **(E)** lymphocytic infiltration in an RAI-administered mouse at 12 months; **(F)** vacuolization with pleomorphism in an RAI-administered mouse at 3 months; **(G)** an unexposed control at 12 months; **(H)** increased fibrosis in an RAI-administered mouse at 12 months. **(A–F)** were stained with hematoxylin and eosin, and **(G, H)** were stained with Masson's Trichrome (scale bar = 100 μm).

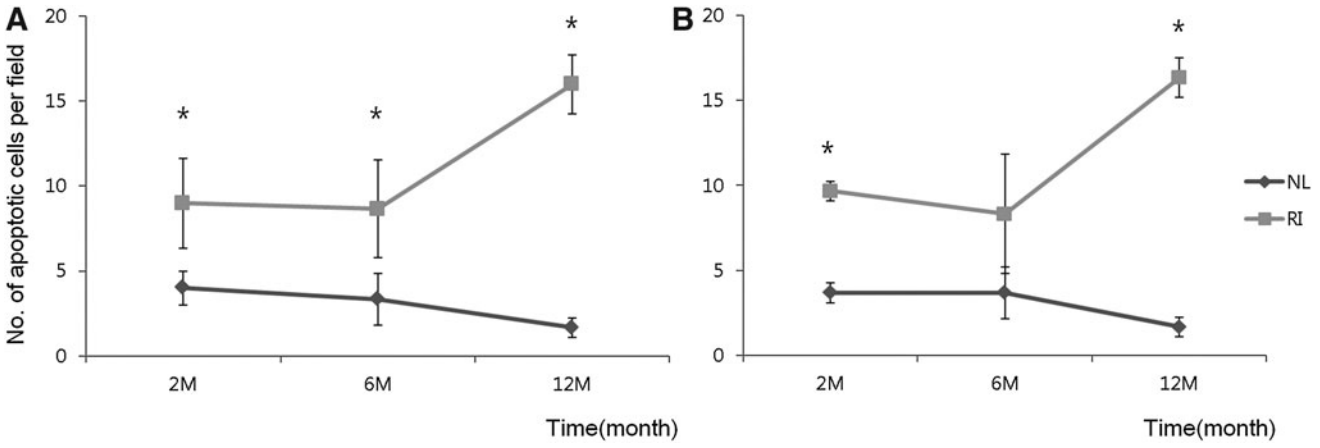

FIG. 4. Quantitative analysis by TUNEL assay. The analysis shows that the numbers of apoptotic cells were greater in the RAI-treated group than in unexposed controls at 2, 6, and 12 months post-treatment. **(A)** The numbers of TUNEL-positive cells per field in acinar cells ($p < 0.001$), and **(B)** the numbers of TUNEL-positive cells per field in ductal cells ($p < 0.001$). The dots and error bars denote means and standard deviations, respectively. The *x*-axis denotes months (M); the *y*-axis, numbers of apoptotic cells per field; and the asterisks, significant points (NL, normal unexposed control group; RAI, RAI-treated group). TUNEL, terminal deoxynucleotidyl transferase dUDP nick end labeling.

In the present study, we performed histopathologic and functional examinations using a murine model of SG dysfunction induced by RAI, and observed both histological and functional changes. RAI-treated mice were lighter than unexposed control mice from 1 to 12 months post-RAI administration, which we attribute to damaged oral health and nutritional insufficiency after RAI exposure. However, it is possible that weight loss was caused by hypothyroidism after RAI administration, as results on this topic are discrepant among species (16–19). The weights of SGs of RAI-treated mice were less than those of unexposed control mice from 1 to 12 months, possibly indicating progressive atrophy.

No significant differences in salivary lag times or SFRs were observed between the two groups at 1 or 2 months post-treatment, but significant differences were found at 3 months, which suggests that 3 months is the minimum time required to observe SG dysfunction objectively by flow testing in our murine model.

Histological changes in SGs after RAI administration were also examined. RAI-treated SGs revealed nonspecific manifestations of cellular injury combined with acinar loss and disorganization, and in some animals, glandular duct enlargement and marked lipomatosis were observed (4,20–22). Furthermore, SGs in RAI-treated mice showed pale cytoplasm, atypical ductal configuration, septal widening, lymphocyte infiltration, cytoplasmic vacuolization with pleomorphism, and increasing fibrosis in tissues.

Apoptosis is considered a possible mechanism of SG damage induced by RAI (20). In the present study, TUNEL assays revealed more apoptotic cells in both acini and ducts in RAI-treated mice, indicating that ductal and acinar cells were damaged by RAI. Nevertheless, further investigation of the mechanisms responsible, including the downstream pathway, for the RAI-induced apoptosis of SG epithelial cells is required.

Salivary scintigraphy is a well-established technique for evaluating salivary function and, in a previous study, confirmed the presence of SG damage by RAI in rabbits (22). However, scintigraphy has not been used in mice because its resolution is too poor to depict organs capable of accumulating iodide. Accordingly, a tomographic technique, such as SPECT, is needed to achieve the level of spatial resolution required (23).

In the present study, we investigated the spatial distributions of the uptakes and excretions of ^{99m}Tc pertechnetate from SGs. The rate of ^{99m}Tc pertechnetate uptake in the RAI-treated group was found to be lower than that in the control group, and the amount of ^{99m}Tc pertechnetate excreted was markedly lower in the RAI group at 1 month post-treatment. At 12 months, the rate of ^{99m}Tc pertechnetate uptake in the RAI group was lower than that in the control group, but the amounts of ^{99m}Tc pertechnetate excretion were similar in the two groups. These results support the view that RAI causes damage to SG acinar and ductal cells at 1 month after treatment, and that at 12 months, acini cell damage persists, whereas ductal cell damage improves with time. This finding also demonstrates that SPECT provides an excellent means of evaluating salivary function in small animal models.

In this study, we performed morphohistometric and functional evaluations of RAI-induced SG dysfunction over 12 months post-RAI treatment using an *in vivo* murine model. To the best of our knowledge, this is the first study to describe SG damage *in vivo* over the long-term. However, this study has some limitations that warrant consideration. First, an RAI dose of 0.01 mCi/g body weight was administered based on a review of related animal studies (0.004–0.0216 mCi/g body weight) (20,24–26). According to our preliminary study, this dose appeared to be sufficient to damage SGs without compromising general health. Nevertheless, additional studies are required to investigate the RAI dose–response relationship, and an appropriate preclinical animal model should be established. Second, our histological study was limited to submaxillary glands because parotid glands are too small to monitor tissue acquisition in the mouse. Third, the most difficult aspect of this study was to manage RAI. Although RAI emits low doses of radiation, examiners can be easily exposed

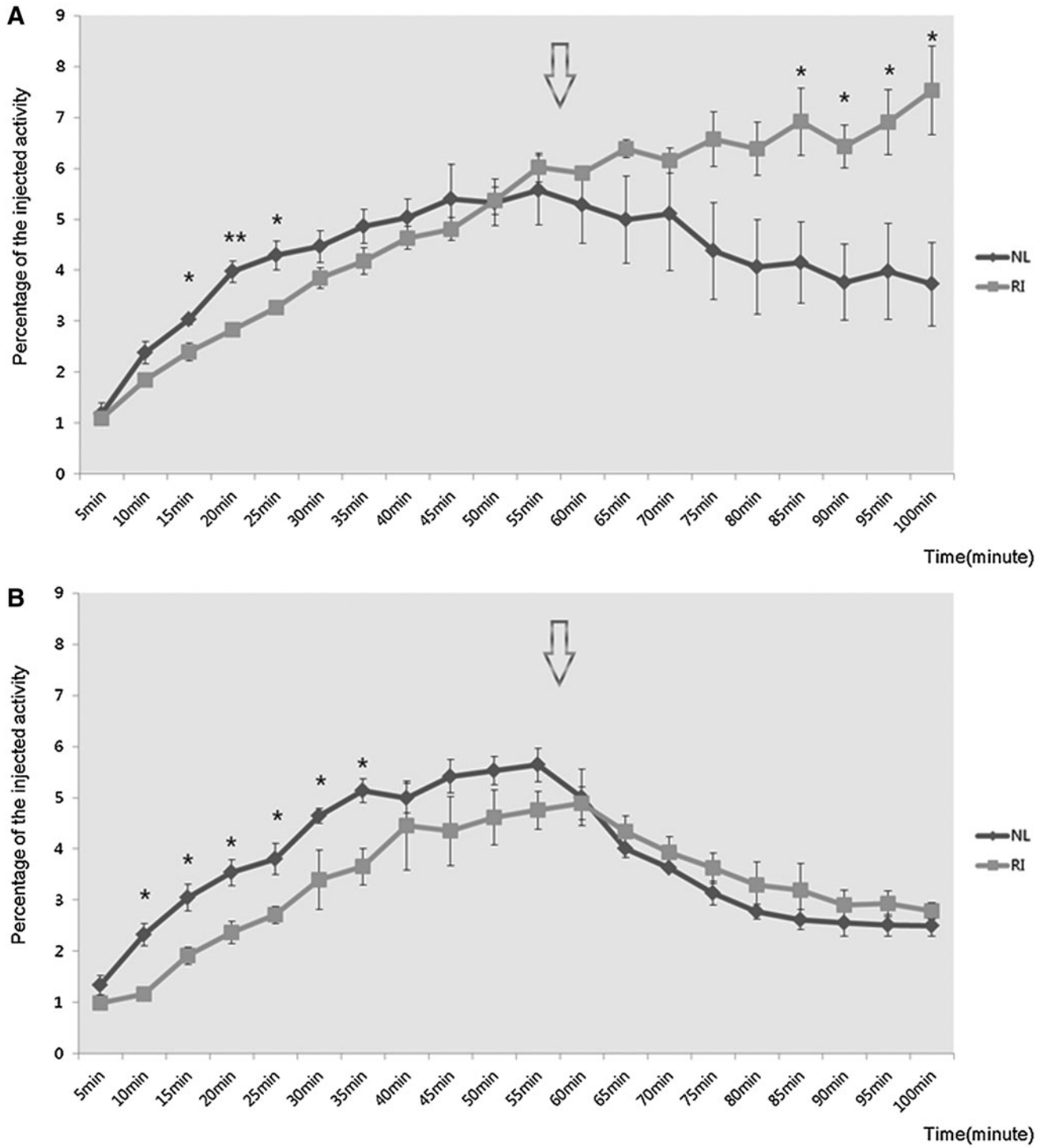

FIG. 5. Dynamics of ^{99m}Tc pertechnetate uptake and excretion at **(A)** 1 month and **(B)** 12 months post-treatment. SG dysfunction in the RAI-administered mice was caused by impaired uptake and marked impairment of excretion at 1 month ($p < 0.001$). SG dysfunction in RAI-administered mice was caused by impaired uptake at 12 months ($p < 0.001$). Arrows indicate the time of pilocarpine injection. Dots and error bars denote means and standard deviations, respectively. The *x*-axis denotes time (minutes); the *y*-axis, percentages of injected activity; and the asterisks, significant points (NL, normal unexposed control group; RAI, RAI-treated group).

to the radioactivity. To avoid direct exposure to RAI, we could not examine the mice contaminated by RAI within 1 month. Because RAI has a half-life of about 8 days, the remaining activity of RAI decreases to less than 12.5% of the initial amount after 1 month. Therefore, all experiments were conducted 1 month after treatment at a time point when radiation was minimal.

In conclusion, various patterns of alterations were observed in RAI-treated mice, that is, body weight loss, SG weight loss, increased salivary lag time, and reduced SFR.

Furthermore, histological changes, including increased apoptosis, and salivary dysfunction by SPECT were observed in RAI-treated mice. We suggest that studies on the mechanism and treatment of SG damage induced by RAI should be performed using the described murine experimental model, because it appears to be appropriate for investigations of SG functional recovery after RAI administration.

Acknowledgments

This research was supported by the Basic Science Research Program through the National Research Foundation of Korea funded by the Korean Ministry of Education, Science and Technology (Grant no. 2012 R1A1A2042632) and by an Inha University research grant.

Author Disclosure Statement

The authors have no potential conflict of interest to declare.

References

1. Albrecht HH, Creutzig H 1976 Salivary gland scintigraphy after radioiodine therapy. Functional scintigraphy of the salivary gland after high dose radioiodine therapy. ROFO Fortschr Geb Rontgenstr Nuklearmed **125:**546–551.
2. Bohuslavizki KH, Brenner W, Wolf H, Sippel C, Toenshoff G, Tinnemeyer S 1995 Value of quantitative salivary gland scintigraphy in the early stage of Sjögren's syndrome. Nucl Med Commun **16:**917–922.
3. Bohuslavizki KH, Brenner W, Lassmann S, Tinnemeyer S, Toenshoff G, Sippel C 1996 Quantitative salivary gland scintigraphy in the diagnosis of parenchymal damage after treatment with radioiodine. Nucl Med Commun **17:**681–686.
4. Bohuslavizki KH, Brenner W, Lassmann S, Tinnemeyer S, Kalina S, Clausen M 1997 Quantitative salivary gland scintigraphy—a recommended examination prior to and after radioiodine therapy. Nuklearmedizin **36:**103–109.
5. Walter MA, Turtschi CP, Schindler C, Minnig P, Müller-Brand J, Müller B 2007 The dental safety profile of high-dose radioiodine therapy for thyroid cancer: long-term results of a longitudinal cohort study. J Nucl Med **48:**1620–1625.
6. Vanhove C, Defrise M, Franken PR, Everaert H, Deconinck F, Bossuyt A 2000 Interest of the ordered subsets expectation maximization (OS-EM) algorithm in pinhole single-photon emission tomography reconstruction: a phantom study. Eur J Nucl Med **27:**140–146.
7. Defrise M, Vanhove C, Nuyts J 2008 Perturbative refinement of the geometric calibration in pinhole SPECT. IEEE Trans Med Imaging **27:**204–214.
8. Ish-Shalom S, Durleshter L, Segal E, Nagler RM 2008 Sialochemical and oxidative analyses in radioactive I131-treated patients with thyroid carcinoma. Eur J Endocrinol **158:**677–681.
9. Spitzweg C, Joba W, Schriever K, Goellner JR, Morris JC, Heufelder AE 1999 Analysis of human sodium iodide symporter immunoreactivity in human exocrine glands. J Clin Endocrinol Metab **84:**4178–4184.
10. Chung JK 2002 Sodium iodide symporter: its role in nuclear medicine. J Nucl Med **43:**1188–1200.
11. Levy O, Vieja A, Carrasco N 1998 The Na^+I^- symporter (NIS): recent advances. J Bioenerg Biomembr **30:**195–206.
12. Smanik PA, Liu Q, Furminger TL, Ryu K, Xing S, Mazzaferri EL 1996 Cloning of the human sodium iodide symporter. Biochem Biophys Res Commun **226:**339–345.
13. Spitzweg C, Heufelder AE 1998 The sodium iodide symporter: its emerging relevance to clinical endocrinology. Eur J Endocrinol **138:**374–375.
14. Baum BJ 1993 Principles of saliva secretion. Ann NY Acad Sci **694:**17–23.
15. Helman J, Turner RF, Fox PC 1987 99mTc-pertechnetate uptake in parotid acinar cells by the $Na^+/K^+/Cl^-$ cotransport system. J Clin Invest **79:**1310–1313.
16. Umezu M, Kagabu S, Jiang J, Sato E 1998 Evaluation and characterization of congenital hypothyroidism in rdw dwarf rats. Lab Anim Sci **48:**496–501.
17. Dixon RM, Reid SW, Mooney CT 1999 Epidemiological, clinical, haematological and biochemical characteristics of canine hypothyroidism. Vet Rec **145:**481–487.
18. Tzotzas T, Krassas GE, Konstantinidis T, Bougoulia M 2000 Changes in lipoprotein(a) levels in overt and subclinical hypothyroidism before and during treatment. Thyroid **10:**803–808.
19. Guyton AC, Hall JE 2000 The thyroid metabolic hormones. In: Guyton AC, Hall JE (eds) Textbook of Medical Physiology, 10th edition. WB Saunders, Philadelphia, pp 858–868.
20. Kutta H, Kampen U, Sagowski C, Brenner W, Bohuslavizki KH, Paulsen F 2005 Amifostine is a potent radioprotector of salivary glands in radioiodine therapy. Structural and ultrastructural findings. Strahlenther Onkol **181:**237–245.
21. Bohuslavizki KH, Brenner W, Klutmann S 1998 Radioprotection of salivary glands by amifostine in high-dose radioiodine therapy. J Nucl Med **39:**1237–1242.
22. Bohuslavizki KH, Klutmann S, Jenicke L 1999 Salivary gland protection by S-2-(3-aminopropylamino)-ethylphosphorothioic acid (amifostine) in high-dose radioiodine treatment: results obtained in a rabbit animal model and in a double-blind multi-arm trial. Cancer Biother Radiopharm **14:**337–347.
23. Franken PR, Guglielmi J, Vanhove C, Koulibaly M, Defrise M, Darcourt J, Pourcher T 2010 Distribution and dynamics of (99m)Tc-pertechnetate uptake in the thyroid and other organs assessed by single-photon emission computed tomography in living mice. Thyroid **20:**519–526.
24. Bohuslavizki KH, Klutmann S, Jenicke L, Kröger S, Buchert R, Mester J, Clausen M 1999 Salivary gland protection by S-2-(3-aminopropylamino)-ethylphosphorothioic acid (amifostine) in high-dose radioiodine treatment: results obtained in a rabbit animal model and in a double-blind multi-arm trial. Cancer Biother Radiopharm **14:**337–347.
25. Bhartiya US, Raut YS, Joseph LJ, Hawaldar RW, Rao BS 2008 Evaluation of the radioprotective effect of turmeric extract and vitamin E in mice exposed to therapeutic dose of radioiodine. Indian J Clin Biochem **23:**382–386.
26. Joseph LJ, Bhartiya US, Raut YS, Hawaldar RW, Nayak Y, Pawar YP, Jambhekar NA, Rajan MG 2011 Radioprotective effect of Ocimum sanctum and amifostine on the salivary gland of rats after therapeutic radioiodine exposure. Cancer Biother Radiopharm **26:**737–743.

Address correspondence to:
Young-Mo Kim, MD
Department of Otorhinolaryngology–Head and Neck Surgery
Inha University School of Medicine
27, Inhang-ro, Jung-gu
Incheon 400-711
Republic of Korea

E-mail: ymk416@inha.ac.kr